ENVIRONMENTAL GEOPHYSICAL SURVEYING AT AN ABANDONED MILITARY BASE (LENTI, SW HUNGARY)

Lénárd PÁL[1], Zsófia SÁRI[2], Brigitta SZABÓ[1]

ABSTRACT:
Environmental geophysical measurements were carried out on the former Bottyán János Military Base in 2009, in order to detect buried installation and possible, pollutants. Specific area (a parking lot and a fuel station of the tanks and armoured personnel carriers, both covered by concrete slabs) of the abandoned military base were surveyed by geomagnetic and ground penetrating radar (GPR) methods. However no buried objects were found, the results reveal the soil structures below the concrete layer, providing useful information about the volume of the artificial filled-in – and possibly polluted – soil, which is the basis of any recultivation work.

Keywords: *geophysical measurements, military base, GPR.*

1. INTRODUCTION

Geophysical measurements were carried out on the former Bottyán János Military Base near Lenti, southwest Hungary in 2009. Lenti is located in Zala County, near the Slovenian border (**Fig. 1**). The location was a base of a motorized combined infantry regiment, later a brigade of the Hungarian Defense Forces, prior to 1994. Since the final abandon of the base in 1997, the place was partly used to accommodate some low-grade industrial activities. The local government of Lenti intends to use the place for tourism, therefore environmental measurements were needed for future recultivation.

Fig. 1 Location map of Lenti

[1] *Department of Geophysics and Space Science, Eötvös Loránd University, Budapest*
[2] *MOL Group*

There were no preceding geophysical measurements at the study area. The research was carried out in a frame of a joint field practice of Eötvös University, Budapest, and the University of Leeds, UK (*Timár et al., 2009*).

The goals of this project were to find buried objects, find and delineate possible pollutants (oil, acid, scrap metal), and investigate the usability of different measurement techniques on the Military Base (*Magyar et al., 1995*). The main measurement areas were the former parking place of the military vehicles and the former fuel station. These objects were constructed of concrete blocks but we could not implement the measurements everywhere. For impounding of the study areas we used the GPS corrected map of the army base (*Sári, 2009*). GPR and geomagnetic measurement methods were used to achieve our goals. These methods are proven to be suitable for roles like this.

The following sections contain the short description of the methods, the measurement techniques, the interpretation of the results, and our conclusions.

2. MEASUREMENT METHODS

2.1. The GPR method

In some cases it can be very useful for detailed structural interpretation of buildings, roadways, pipelines or the soil characteristics in the shallow subsurface. Using the Ground Penetrating Radar (GPR) method we can take a high-resolution image of these structures.

The GPR consists of a transmitter and a receiver. The transmitter sends a microwave signal (radar wave) to the test range, for example to the subsurface. The spreading of this electromagnetic signal depends on the relative permittivity, magnetic permeability and the specific conductivity of the subsurface. Most of the Earth's materials are non-magnetic, so we can take the permeability of vacuum (μ_0). If the relative permittivity changes, the radar waves are reflected to the surface. The travel time of the reflected wave is related to the depth of the reflector, hence we can get information about structural variations under the surface.

The frequency range of the microwave signal (of the transmitter) is 100 Hz-1 GHz. Frequency is inversely proportional to the depth of penetration. It means that higher frequency range gives us shallower penetration. We also have to take into account that this higher frequency is related to a smaller wavelength, so it enhances the resolution of our measurement. So choosing the best GPR antenna is critical point of the measurements.

The permittivity of the medium is ε:

$$\varepsilon = \varepsilon_r \varepsilon_0 \tag{1}$$

where ε_r is the relative permittivity and ε_0 is the permittivity of vacuum.

$$\varepsilon_r = \frac{\varepsilon}{\varepsilon_0} = k \tag{1a}$$

where k is the dielectric constant. This parameter defines the index of refraction of the medium and it controls the velocity of radar waves in the material:

$$v = \frac{c}{\sqrt{k}} \tag{2}$$

where c is the speed of light in air and v is the velocity of the wave in the subsurface medium (*Cardimona et al., 2006*). **Table 1** shows the typical dielectric constants and the velocity values of some common materials.

Table 1. ***The velocity of some material***

Material	Typical dielectric const.	Velocity (m/ns)
air	1	0.30
water	81	0.033
dry sand	4-6	0.15-0.12
sandstone	4	0.14
granite	9	0.10

In the interest of proper interpretation, basic data processing needed, which usually consists of the following steps (*Milson, 2003*):

1. Zero-time adjust
2. Automatic Gain Correction
3. Frequency filtering
4. Deconvolution
5. Migration

Buried objects under the surface cause changes in the permittivity. Such changes appear on the image as hyperboles. By the analysis of these features we can draw conclusions upon the velocity of the waves. **Fig. 2** shows a 400 MHz GPR profile.

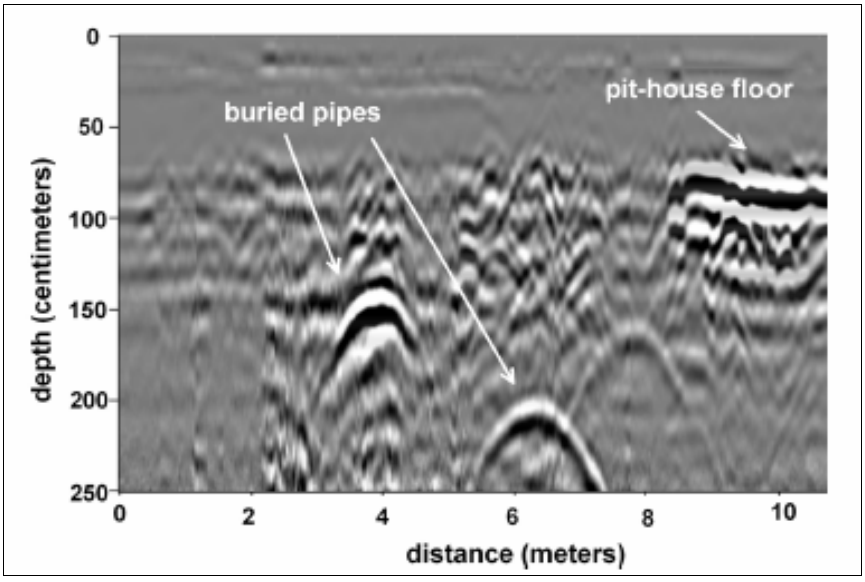

Fig. 2 A 400 MHz profile across a pithouse floor. Reflection hyperboles represent buried water pipes (*Conyers, 2002*).

2.2. The geomagnetic method

The magnetic research method is based on the magnetic properties of the materials. These properties divide the materials into five common groups. These are: dia- , para-, ferro-, antiferro- and ferrimagnetic materials.

The most important physical parameter is the magnetic susceptibility (κ). By this parameter we can define the magnetization, to which the respond of the material for a given magnetic field is related. It is described by the following equations:

$$\underline{J} = \kappa \cdot \underline{H} \tag{3}$$

$$\underline{B} = \mu_0 \cdot (\underline{H} + \underline{J}) \tag{4}$$

where J represents the magnetization, H is the strength of the magnetic field and B is the vector of magnetic induction. From these equations then we can deduce the contact between magnetic susceptibility and permeability:

$$\mu_r = 1 + \kappa \tag{5}$$

Table 2 shows the susceptibility value of some minerals. In case of diamagnetic materials the direction of J is reverse to H. The magnetization vector of a paramagnetic material has the same orientation as H. Using this method subsurface magnetic materials e.g. volcanic rock (basalt) blocks and man-made objects can be studied.

Table 2. ***Susceptibility value of some ores***

Diamagnetic	Quartz	-1,63
	Calcite	-1,38
	Water	0-90
Paramagnetic	Siderite	250-800
	Pyrite	120
Antiferro-magnetic	Hematite	200-1500
Ferrimagnetic	Magnetite	$8 \cdot 10^5$-$2 \cdot 10^6$

The measurements were carried out using GSM-19 Overhauser magnetometer. The operating principle of this magnetometer is nearly the same as in the case of the proton precession magnetometer. Unbound electrons in the liquid transfer energy to the hydrogen nuclei, therefore polarize the liquid. In view of the precession frequency, the strength of the magnetic field can be determined.

$$f_P = \gamma_P \cdot \frac{|\underline{B}|}{2\pi} \tag{6}$$

where γ_p is the proton precession gyromagnetic constant and f_p is the frequency of precession.

The raw data of geomagnetic measurements have to be processed before interpretation. The usual processing workflow consists of three main steps, which are the following (*Milson, 2003*):

1. Base correction: eliminates diurnal variations of the magnetic field of the Earth.
2. Reduction to the pole: recalculates total magnetic intensity data as if the inducing magnetic field had an inclination of 90^{o}.
3. Mapping: generation of gradient and H maps of the survey area.

3. THE SURVEY SITES

3.1. The parking

In this area geomagnetic method was applied, using three Overhauser magnetometers. One of them was the base magnetometer and two others were used for the measurements. Base correction was applied to the registered data. The reduction to the pole was not implemented, as we wanted to know only the location of anomalous features, and the anomalies on the corrected map were less significant.

Fig. 3 shows the magnetic gradient map of the parking. South of the area shows fewer anomalies, while ont he northern part systematic anomalies were found. Most of the map represents surface objects, such as a concrete drain in the middle and remnants of ferro-concrete pillars in the north.

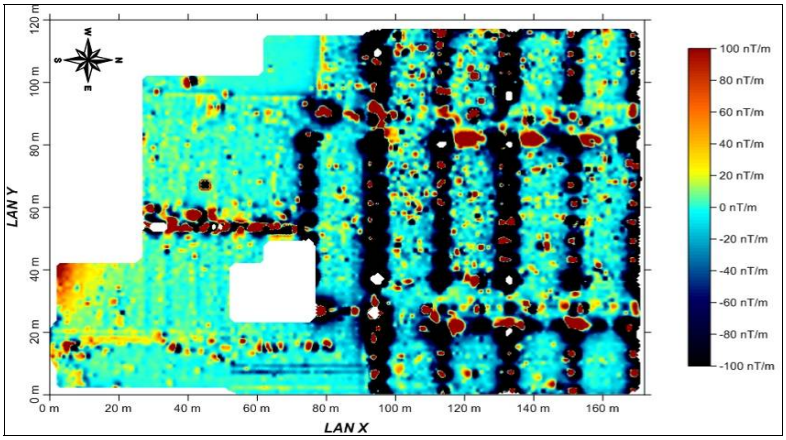

Fig. 3 The magnetic gradient map of the parking

The two parallel lines on the bottom were assumed to be pipes. The GPR measurements did not indicate this feature. Therefore, it was measured with the magnetometers crossline. These two measurements made us to reject the original idea. Possibly it was an error in the first magnetic measurement.

GPR measurements were done only in the eastern part with 0.5 m spacing between the lines at 500 MHz frequency (**Fig. 4**). Around the pillars no significant information was given by the GPR. However, in front of the ramp (to the east) the anomalies in the radar timeslices could be well-correlated with the edge of the concrete slabs. The large-scale anomalies are in line with the magnetic ones, and reperesent the original morphology (*Sári, 2009*).

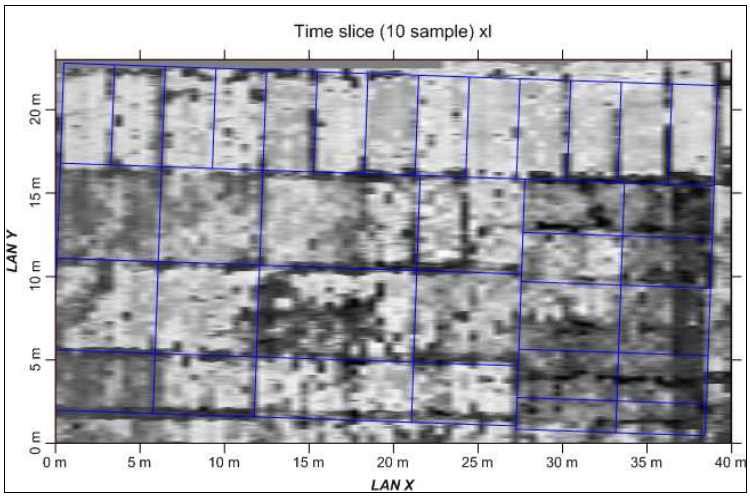

Fig. 4 A GPR time slice of the parking covered by the map of the concrete blocks (f=500 MHz)

3.2. The fuel station

The second place was the former fuel station for army vehicles. In the middle of the place there is a 0.5 m high ramp. The whole area is covered by asphalt and surrounded by lightning rods. Thus the magnetic method was found to be unsuitable, only GPR was applied. The measurements were carried out by two types of instruments (**Fig. 5**): a Zond-e 12 GPR with 500 MHz and 1GHz antennas, and a PULSEKKO with variable frequencies.

Fig. 5 GPR instruments: the Zond-e 12 GPR with a notebook on it (left), and the central unit of PULSEKKO

The structure of the two instruments is different. The previous has a fixed antenna, and is controlled by a notebook, while in the case of the latter instrument the frequency can be adjusted, and the instrument itself controls the measurement and saves the data. The data processing and interpretation was made by Prism 2D, Prism 3D, and ReflexView programs.

Near the 0.5 m high ramp the measurement was not feasible. The rest of the site was measured both at 500 MHz and 1 GHz frequencies. At the same time, the PULSEKKO GPR had been tested by measuring points along a given line while steadily moving from the center point.

Comparing of the two with 500MHz measured sections of the two instruments was turned out, that perfectly identical sections can be measured with them, so the measuring group has been able to work in parallel on the parking area, thus a larger surface area has been assessed.

Interpolated data are shown in the profiles on/in place of ramp (**Fig. 6**). The identified bottom of filling was selected during the interpretation on each section. The surface of the bottom of filling was generated in depth scale instead of time scale by using estimated dielectric constant from resulting time data. The depth of surface is changing between 0.5 m and 1.2 m. The surface of the bottom of the concrete slabs is also clearly visible reflector. The resulting surfaces will be used for computing the volume of the filling and the concrete layer.

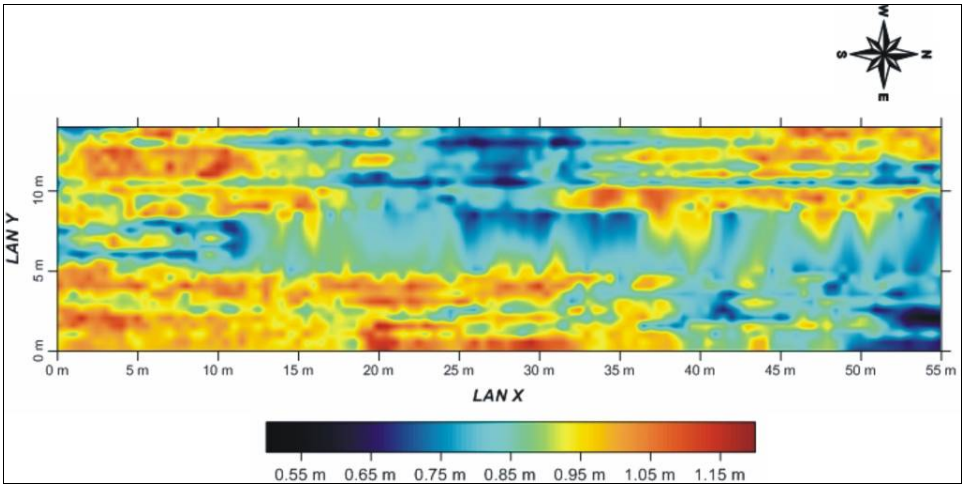

Fig. 6 The generated surface of the base of the filling-up. The colours represent the depth of the surface at a given point.

4. ESTIMATION OF THE VOLUME OF DISTURBED SOIL UNDER THE CONCRETE SLABS

One of our aims was to estimate the thickness of the concrete layer and the mass of the filling-up. First the base of the filling-up was picked on GPR images, then the data of this horizon were interpolated.

The estimated value of the permittivity was determined from the hyperbolas. Three different models were used to estimate the thickness and volume of the filling-up. For the first model the permittivity was the estimated mean value and the other two models were built using the mean value of permittivity ± 0.15. This caused the changes in depth of the horizon in the different models (**Fig.7**).

First, the depth of the horizon was computed with different values of ε, then, the common volume of the filling-up and the concrete slabs was computed. Then the volume of concrete was substracted from the calculated values (we assumed the thickness of the concrete layer being 20 ± 3 cm).

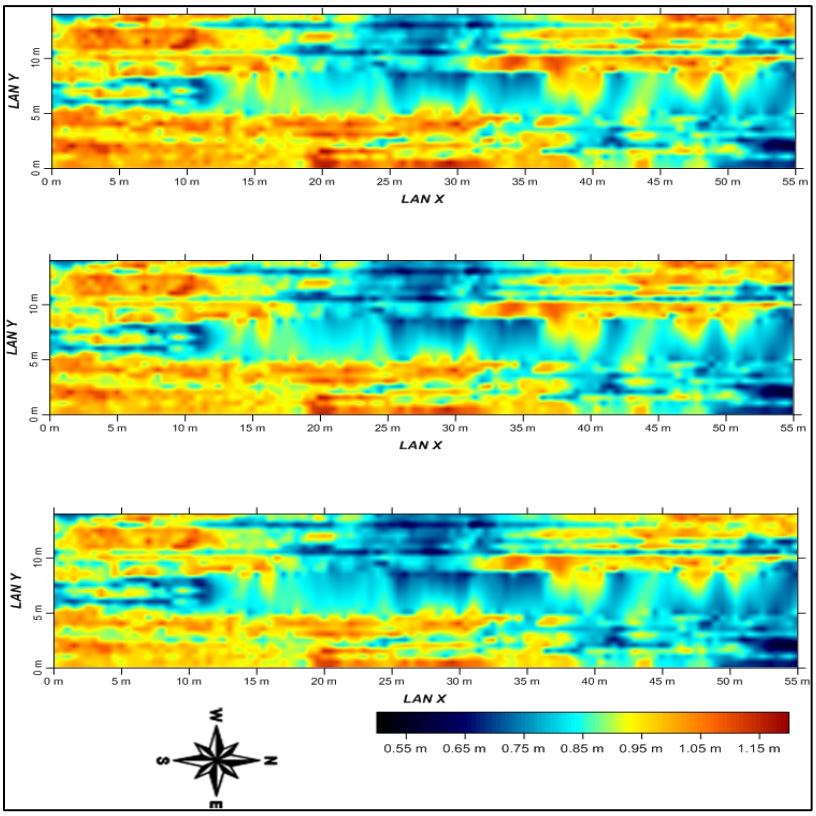

Fig. 7 Variations of horizon depth by permittivity. The permittivity values are 4 (top), 4.15(middle) and 4.3(bottom)

Table 3. ***Results of volume calculations***

	Fuel station	**Parking**
Thickness of concrete (cm)	20 ± 3 cm	20 ± 3 cm
Volume of concrete (m^3) (number of trucks)	212 ± 12.2 % 17.67 ±2,55	4128 ± 17.65 % 344 ± 60.72
Volume of filling-up (m^3) (number of trucks)	529.73 ± 3.3 % 44.14 ± 1.46	14222 ± 6.5 % 1185.17 ± 77.04

The potential errors of the preliminary estimations can be derived from several sources. Field observations and GPR surveys showed that the thickness of the concrete slabs fluctuated ± 3 cm. Interpretation mistakes can be made while picking the horizon, which can cause ± 10 cm changes in depth. The changes of permittivity results a 1.6% relative error.

The following table summarizes the results of our estimations. The calculations were made for both the survey sites. The volumes are given in m^3 and in the number of the usual Russian Kamaz trucks needed for the transport (one load is approximately 12 m^3). In case of the fuel station the thickness of the concrete slabs caused relatively higher deviation of the volumes.

5. CONCLUSIONS

It can be established that the combination of GPR and geomagnetic methods is effective for such environmental surveys. Magnetic anomaly maps were used to impound ferrous objects, and were also useful as basemaps of the survey sites. GPR measurements had helped to identify anomalies of morphological origin. The horizontal and vertical extent of anomalies could be determined. GPR measurements provided a good basis for volumetric calculations. Our data did not indicate subsurface objects.

For future recultivation, further investigations are suggested. Shallow coring can significantly improve the precise thickness of the filling-up, which is the most uncertain factor among the parameters used for our volumetric estimation (*Galsa, 1997; Drahos and Galsa, 2007*). In addition, samples taken from the core can be analysed. It can provide information on the extent of contaminations in the subsurface layer. With these considerations the necessity of soil replacement during the recultivation can be more precisely constrained.

REFERENCES

Cardimona S., Webb D., Lippincott A., (2006), *Ground Penetrating Radar. Proc., First International Conference on the Application of Geophysical and NDT Methodologies to Transportation Facilities and Infrastructure*, St. Louis, Mo., Dec. 2000. URL: http//www.umr.edu/2006geophysics/hgconproceedings/2000papers/index.htm.

Conyers L. B., (2002), *Ground-Penetrating Radar, Encyclopedia of Imaging Science and Technology*, pp. 131-159. Wiley Online Library, URL: http://onlinelibrary.wiley.com/book/10.1002/0471443395

Drahos D., Galsa A., (2007), *Penetrációs elektromos szonda modellezése véges elemes numerikus módszerrel*, Magyar Geofizika, 48 (1), pp. 22–30.

Galsa A., (1997), *Felszín alatti vízmozgás modellezése egy alföldi szelvényen, fúrólyukban mért víznyomások felhasználásával*, Magyar Geofizika, 38 (4), pp. 245–256.

Magyar B., Stickel J., Verő L., Pádár I., (1995), *Assessment and remediation of environmental damage in the abandoned Soviet military bases in Hungary. Assessing and Managing Health Risks from Drinking Water Contamination: Approaches and Applications* (Proceedings of the Rome Symposium, September 1994). IAHS Publ. no. 233, 1995. pp. 255-266.

Milson J., (2003), *Field Geophysics*. Wiley, Chichester, 232 p.

Sári Zs., (2009), *Környezetgeofizikai kutatások a Lenti melletti katonai bázison -Terepgyakorlati jelentés*. ELTE Geofizikai és Űrtudományi Tanszék, 13p.

Timár G., Székely B., Zámolyi A., Houseman G., Stuart G., Grasemann B., Dombrádi E., Galsa A., Spahic D., Draganits E. and the ELTE-Leeds-UniWien Workgroup Team, (2009). *Neotectonic implications by geophysical surveys of topographic features identified by Airborne Laser Scan-ning in the Neusiedlersee/Ferto area* (Austria/Hungary), Geophysical Research Abstracts, 11, 9240.